Rapid Prototyping J

Erosion Characteristics on Surface Texture of Additively Manufactured AlSi10Mg Alloy in SiO2 Quartz Added Slurry Environment

Journal:	*Rapid Prototyping Journal*
Manuscript ID	RPJ-10-2021-0283.R1
Manuscript Type:	Original Article
Keywords:	Additive manufacturing, AlSi10Mg, Quartz sand, Slurry erosion, Surface roughness

Erosion Characteristics on Surface Texture of Additively Manufactured AlSi10Mg Alloy in SiO2 Quartz Added Slurry Environment

Abstract

Purpose: Additive manufacturing, also known as 3D manufacturing, is the process of manufacturing a part designed in a computer environment using different types of materials such as plastic, ceramic, metal, or composite. Similar to other materials, aluminum alloys are also exposed to various wear types during operation. Production efficiency needs to be aware of its reactions to wearing mechanisms.

Design/ Methodology/ Approach: In this study, quartz sands (SiO_2) assisted with oxide ceramics were used in the slurry erosion test setup and its abrasiveness on the AlSi10Mg aluminum alloy material produced by the 3D printer as Selective Laser Melting (SLM) technology was investigated. Quartz was sieved with an average particle size of 302.5 µm and a slurry environment containing 5%, 10%, and 15% quartz by weight was prepared. The experiments were carried out at the velocity of 1.88 m/s (250 rpm), 3.76 m/s (500 rpm), and 5.64 m/s (750 rpm) and the impact angles 15°, 45°, and 75°.

Findings: With these experimental studies, it has been determined that the abrasiveness of quartz sand prepared in certain particle sizes is directly related to the particle concentration and particle speed and that the wear increases with the increase of the concentration and rotational speed. Also, the variation of weight loss and surface roughness of the alloy was investigated after different wear conditions. Surface roughness values at 750 rpm speed, 10% concentration, and 75 ° impingement angle are 0.32µm and 0.38 µm for 0 ° and 90 ° samples, respectively, with a difference of approximately 18%. Moreover, concerning a sample produced at 0 °, the weight loss at 250 rpm at 10% concentration and 45 ° particle impact angle is 32.8 mg, while the weight loss at 500 rpm 44.4 mg, and weight loss at 750 rpm is 104 mg. Besides, the morphological structures of eroded surfaces were examined using SEM (Scanning Electron Microscope) to understand the wear mechanisms.

Keywords: Additive manufacturing, AlSi10Mg, Quartz sand, Slurry erosion, Surface roughness.

Paper type- Research paper

1. Introduction

According to the ASTM (American Society for Testing and Materials) standard F2792-1, additive manufacturing is the process of combining materials, often in layers on top of each other, to make objects from 3D model data, as opposed to subtractive manufacturing methodologies such as traditional machining (Du *et al.*, 2019; Szymczyk *et al.*, 2020). Production technologies are known as three-dimensional (3D) manufacturing or additive manufacturing have a wide range of uses. Therefore, many companies and research institutions commonly use additive manufacturing methods instead of traditional methods (Łyczkowska *et al.*, 2014; Singla *et al.*, 2021). Due to the advantages, additive manufacturing has widespread use that ensures the rapid development of the filament, materials, and techniques (Lifton *et al.*, 2021). Additive manufacturing methods are opposite of conventional machining methods. In machining, the chips are removed from the base material and a product of the desired shape and size is obtained, while in additive manufacturing, the parts are combined in layers (Ramoni *et al.*, 2021; Waqar, Guo, *et al.*, 2021). Therefore, the use of materials in additive manufacturing is less than traditional machining (Rautio *et al.*, 2020; Zhang *et al.*, 2021). In additive manufacturing methods, materials such as metal, ceramic, plastic, composite can be used, as well as specific production materials(Gupta *et al.*, 2020; Waqar *et al.*, 2020). In addition to its wide range of materials, its use is increasing day by day as it enables the production of parts with very complex geometries with minimum material loss (Waqar, Sun, *et al.*, 2021). Many materials such as ABS (Acrylonitrile Butadiene Styrene), plastic, polyamide (nylon), glass-filled polyamide, stereolithography materials (epoxy resins), silver, titanium, steel, aluminum, wax, photopolymers, and polycarbonate can be used as consumables materials in 3D printers (Damodaran *et al.*, 2021; Le *et al.*, 2017). It enables green production as it is easier to use environmentally friendly and ecologically friendly materials in additive manufacturing (Kurzynowski *et al.*, 2020). The concept of "green production", which is becoming increasingly important today, is important for a more livable future. Green production is the renewal of production steps and the use of environmentally friendly methods and materials in production. The use of less natural resources by the workforce, less waste and pollution, and the recycling of products can be considered within the scope of green production (Farooque *et al.*, 2019; Junjun *et al.*, 2018). Aluminum is the most

abundant element in the world after silicon and oxygen. About 8% of the elements in the earth's crust are aluminum and its compounds. Aluminum and its alloys, due to its many advantages such as being abundant in nature, easy to obtain, low weight, suitable mechanical properties (having a high strength/weight ratio) (Manjunath Patel *et al.*, 2020), high thermal and electrical conductivity, resistance to odor and chemicals, recyclability (Vargel, 2020). Various aluminum metal powder mixtures such as AlSi10Mg (Xu *et al.*, 2021), AlSi7Mg (Wang *et al.*, 2019) and AlSi12 (Xi *et al.*, 2018) are used in metal additive manufacturing technologies depending on the desired product properties (Aboulkhair *et al.*, 2017, 2019). SLM (selective laser melting) production technique used in this study is similar to SLS (selective laser sintering) and the only difference is that the powder is melted instead of sintering with this method (Tawfik *et al.*, 2019; Zhang, Liu, *et al.*, 2018). With the SLM method, complex 3D models can be produced in layers within a few hours (Olakanmi, 2013; Olakanmi *et al.*, 2015). Cobalt-chrome, stainless steels, Inconel, titanium, and aluminum powders can be used as raw materials. It is a great technology for specific productions. Regardless of the method used, every material must have a certain wear resistance (Chawla and Shen, 2001). Wear is a situation that directly affects the life of the equipment in the plants. There are many types of wear and one of the most common problems is an erosive wear (Bansal *et al.*, 2020; Fouad *et al.*, 2011; Venter *et al.*, 2020). About erosive wear, there are also many different wear types (Raadnui, 2021; Saleh *et al.*, 2021; Verma, 2020). Slurry erosive wear is one of these wear types and occurs especially in liquid environments containing a certain quantity of solid particles (Heshmat and Abdelrhman, 2021; Kumar *et al.*, 2020). The facilities where this type of wear is most common are the facilities where quartz sand (Chen *et al.*, 2020; Matikainen *et al.*, 2019), which is a raw material for glass and ceramic, is occurred. SiO2 is displayed when talked about glaze chemistry in pottery. An oxide contributed by many ceramic materials such as all clays, feldspars and frits. Quartz or silica powder is almost 100% SiO2. However, quartz sand of SiO2 is completely different from feldspar SiO2. In the latter, it chemically binds to Al2O3 and also other oxide ceramics. These quartz sands are pumped to manufacturing plants with high amounts of water by using pumps. The equipment on the line is exposed to slurry erosive wear and worn out in a short time (Clark and Llewellyn, 2001; Ojala *et al.*, 2016). Some current studies on AlSi10Mg alloy produced with SLM technology and also combined with slurry wear type are summarized below and no studies on slurry wear with oxide ceramic assisted SiO2 quartz sands have

been found. Li et al. investigated the building orientation on the tensile properties of additively manufctured AlSi10Mg alloy produced with SLM (Li *et al.*, 2021). Atzeni et al. examined the applicability of the abrasive fluidized bed (AFB) method as a finishing process on AlSi10Mg alloyed surfaces produced by direct metal laser sintering (DMLS) (Atzeni *et al.*, 2016). Brandl et al. investigated the microstructure, high cycle fatigue (HCF), and breakage behavior of AlSi10Mg samples produced and processed by the selective laser melting (SLM) method. (Brandl *et al.*, 2012). Hadadzadeh et al. investigated the effect of the building orientation for AlSi10Mg alloy produced by direct metal laser sintering (DMLS) on the columnar to coaxial transition (CET) behavior. (Hadadzadeh, Amirkhiz, Li, *et al.*, 2018). Nurel et al. applied Split Hopkinson Pressure Bar (SHPB-PHC) tests to AlSi10Mg alloy samples produced by the SLM method to investigate their dynamic properties. (Nurel *et al.*, 2018). There are much more studies in the literature about AlSi10Mg alloy produced with SLM as shown in Table 1. Most of these studies are about the determination of mechanical properties, fatigue properties, dynamic behaviors and corrosion types (Beevers *et al.*, 2018; Cabrini *et al.*, 2016; Hadadzadeh, Amirkhiz, Odeshi, *et al.*, 2018; Maconachie *et al.*, 2020; Zhang, Zhu, *et al.*, 2018). Moreover, about the slurry wear process, Patel et al. (Patel *et al.*, 2018) studied on microstructural analysis and wear behaviour after slurry erosion tests for A2024- SiC-ZrSiO4 metal matrix composites. The author indicated that the weight loss increased with increasing rotational speed and supported this situation with microstructural changes. Fals et al. (Fals *et al.*, 2020) examined the slurry wear resistance of AISI 1020 steel which is thermally sprayed deposited with Nb2O5 and Nb2O5+WC12Co coating. The researchers verified that this specific coating condition increases the slurry wear resistance of the mentioned steel. There are lots of study about slurry wear tests, however, there is no study in the literature about the quartz sand (SiO2) assisted slurry-erosive wear of AlSi10Mg alloy produced with AM by using SLM technology. This study is needed to fill this gap in the literature and to examine the erosive wear capability of this current material in different environments. The novelty of the study is the use of SiO2 quartz sands assisted by oxide ceramics in different concentrations for the slurry erosion test setup and the investigations on erosive wear resistance of AlSi10Mg alloy manufactured by AM.

Table 1. Literature studies about SLMed AlSi10Mg

Material and Building Directions	**Aim of the study**	**Authors**

Single directional of pure-AlSi10Mg and nano additive AlSi10Mg	Investigation of the mechanical properties	(Wang and Shi, 2020)
Single directional of carbon-AlSi10Mg	Assessment of the mechanical and electrical properties	(Zhao *et al.*, 2016)
Three directional of SLMed AlSi10Mg	Evaluation of the mechanical and sliding wear properties	(Kan *et al.*, 2021)
Single directional of untreated-AlSi10Mg and T6 heat treated-AlSi10Mg	Investigation of the hardness, tribological and corrosion properties	(Wei *et al.*, 2021)
Four directional of SLMed AlSi10Mg	Study of the fatigue and crack behaviour	(Xu *et al.*, 2021)
Two directional of SLMed AlSi10Mg	Assessment of the microstructure and void dependence of tensile properties	(Ben *et al.*, 2020)
Single directional of SLMed AlSi10Mg	Investigation of the mechanical properties in three different melting mode transition	(Wu *et al.*, 2021)
Two directional of SLMed AlSi10Mg	Effect of T6 treatment sliding against ceramic and steel	(Kan *et al.*, 2021)
Single directional of SLMed AlSi10Mg	Plasma electrolytic oxidation treatment on corrosion and sliding wear performances	(Liu *et al.*, 2021)
Single directional of SLMed AlSi10Mg	Melt spreading behavior, microstructure evolution and wear resistance	

2. Materials and methods

2.1. Preparation of abrasive particles and slurry

The oxide ceramics assisted quartz sands were used as the abrasive material. The measurement of particle size distribution is necessary to determine the percentage of particles in the sample of different size ranges. A dry sieve analysis can be used to determine the particle size distribution. Representing the abrasive sample, a sample is taken from the sample and sifted through a series of sieves. Standard quantity percentages are calculated by weighing the samples held in each sieve (More *et al.*, 2014). In this study, the dry sieve method was applied as clearly stated in the literature. Before weighing, the sample was carefully dried and dehumidified. Percentage distributions of particle sizes were obtained and it was determined that approximately 60% of them were between 180 µm and 425 µm (Table 2). Abrasive particles with an average particle size of 302.5 µm were prepared by sieving the abrasive in sieves with 425 µm and 180 µm openings, respectively. The chemical composition obtained in the XRF (X-Ray Emission Spectroscopy) device of ARL Advant in Table 3 and the SEM images before and after the sieving process in Figure 1 are given. As seen in the SEM image, the abrasive particles used have sharp edges and irregular geometry.

Table 2. Dimensional distribution results according to the sieving process performed following ASTM E 11:82 standard.

Sieve Opening (µm)	Weight (gr)	Differential (%)	Cumulative Under the Sieve (%)
+600	0.25	0.22	100.00
-600 +500	3.21	2.87	99.78
-500 +425	8.16	7.29	96.91
-425 +355	12.14	10.84	89.63
-355 +180	55.35	49.42	78.79
-180 +150	12.12	10.82	29.37
-150 +106	13.43	11.99	18.54
-106	7.34	6.55	6.55
Total	**112.00**	**100.00**	**-**

Table 3. Chemical composition of oxide ceramic assisted quartz sand sample

	SiO_2	CaO	Al_2O_3	MgO	Fe_2O_2	K_2O	TiO_2	Other
Quantity (wt %)	98.3	0	0.74	0.04	0.0065	0.27	0.12	0.5235

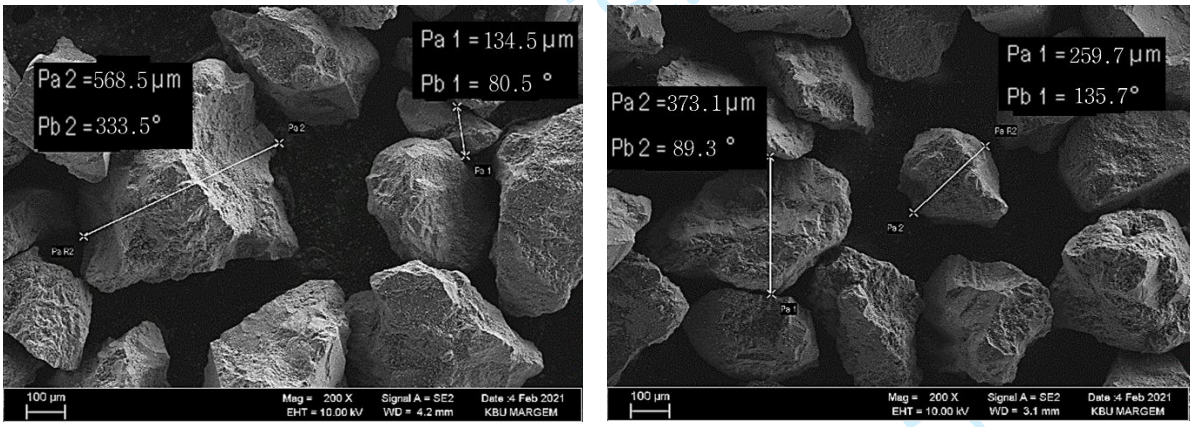

(a) **(b)**

Figure 1. SEM image of quartz sample a) before sieving process b) after sieving process

2.2. Fabrication of samples

In this study, AlSi10Mg test specimens were produced at 0° and 90° building orientations by using a Concept Laser branded Mlab 200R 3D metal printer performed with Selective Laser Melting (SLM) technique by Form Additive Corporation (Figure 2). AlSi10Mg powder (30 µm size) mixture with code "EOS art-no 9011-0024" was used in the

production and chemical composition of the powders is shown in Table 4. No heat treatment has been applied to the test samples. Finally, the sanding process was performed to the additively manufacture AlSi10Mg alloys. The optical microscope images of the samples with 0° and 90° building orientations are given in Figure 3. The etching process before taking the optical images, the samples were etched by the solution of 190 mL H_2O + 5 mL HNO_3 + 3 mL HCl + 2mL HF with a duration of 60 sec.

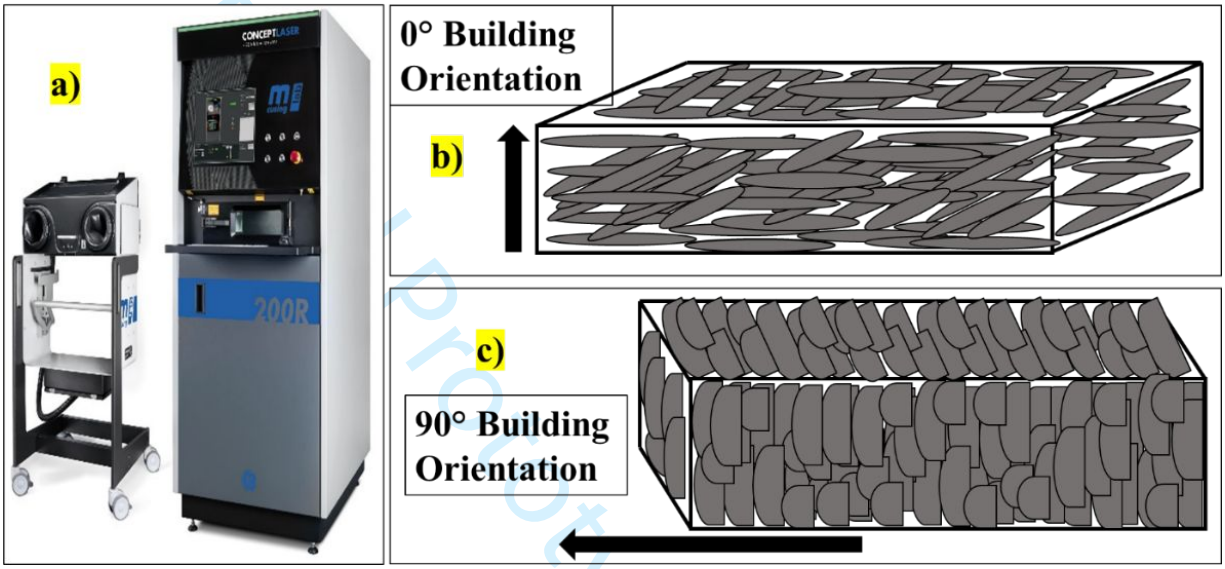

Figure 2. AlSi10Mg alloy, a) printer, b) 0° building orientations, c) 90° building orientations

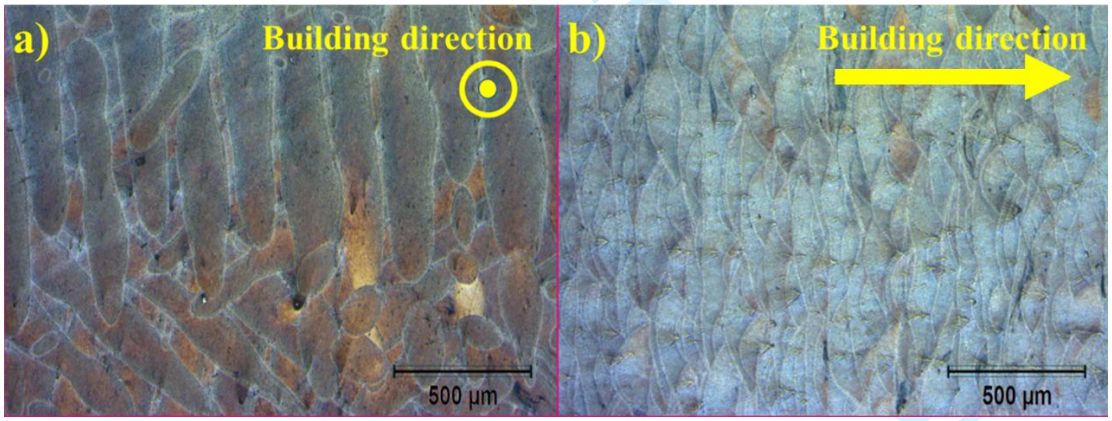

Figure 3. Optical microscope images of the samples with building direction of, a) 0°, b) 90°

Table 4. The chemical composition of the AlSi10Mg powders.

Si (9.0 - 11.0 wt-%)	Fe (0.55 wt-%)	Cu (0.05 wt-%)
Mn (0.45 wt-%)	Mg (0.2 - 0.45 wt-%)	Ni (0.05 wt-%)
Zn (0.10 wt-%)	Pb (0.05 wt-%)	Sn (0.05 wt-%)
Ti (0.15 wt-%)	Porosity (0,15 wt-%)	Al (Balanced)

Before starting the slurry erosion test, the surfaces were sanded with 1200 grit silicon carbide emery paper. With this process, specimens have similar surface roughness values were tried to be prepared. At the end of the sanding, it is aimed to compare the final conditions of the surfaces of the materials exposed to slurry erosion. The surface images of both specimens after the sanding process are given in Figure 4. Besides, the hardness and roughness values of the surface of the specimens are given in Table 5.

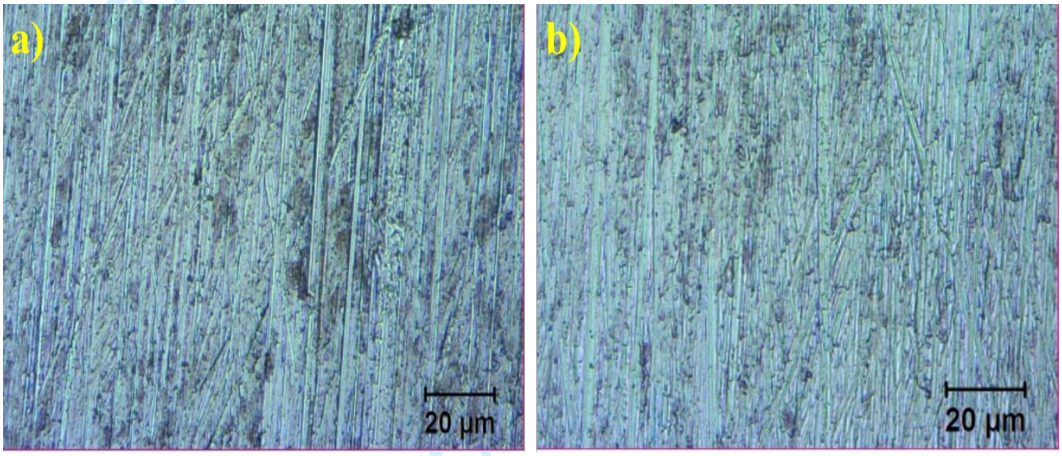

Figure 4. Surface images of specimens after sanding a) 0° , b) 90°

Table 5. Hardness and roughness values of the surface of the specimens

Building direction of the Specimens	0°	90°
Hardness [HV-100kgf]	132	130
Ra [µm]	0.08	0.082

2.3. Slurry erosion experiments

Slurry erosion is generally defined as the removal of material from contact surfaces by solid particles in the liquid environment. This environment is not only liquid but also gas fluid. The experimental setup was designed to test the parameters affecting slurry erosion (Figure 5). It is on the same principle as the experimental setup designed by (More *et al.*, 2014). There are a total of six plates in the chamber, which have an inner diameter of 240 mm and a volume of 10 lt. At the bottom of the chamber, there is a four-bladed mixing propeller as seen in Figure 5a. This mixer is driven by an AC motor with 1.1 kW power, using a belt-pulley mechanism. Samples are connected to the system with the help of sample holders. The sample holders are attached to the arm holder using the arms as seen in Figure 5.b, and the handle holder to the shaft. This shaft is rotated around its axis using a belt-pulley mechanism with another AC motor with 1.1 kW power. Due to the rotational movement around this axis and the adjustable position of the sample holders, the contact

of the quartz particles with the sample can be at different impact angles. Sample holders, arms, and cylindrical arm holders to which the arms are connected are made of stainless steel material for long life. In the wear measurements, the erosion occurring in these sample holders was not taken into consideration, and the same sample holders were used in many tests. The rotation radius (R) of the holders attached to the sample arms is 72 mm in Figure 5c. Samples are 30 x 5 x 6 mm in size. The surface size exposed to erosion is 30 x 5 mm as seen in Figure 5d.

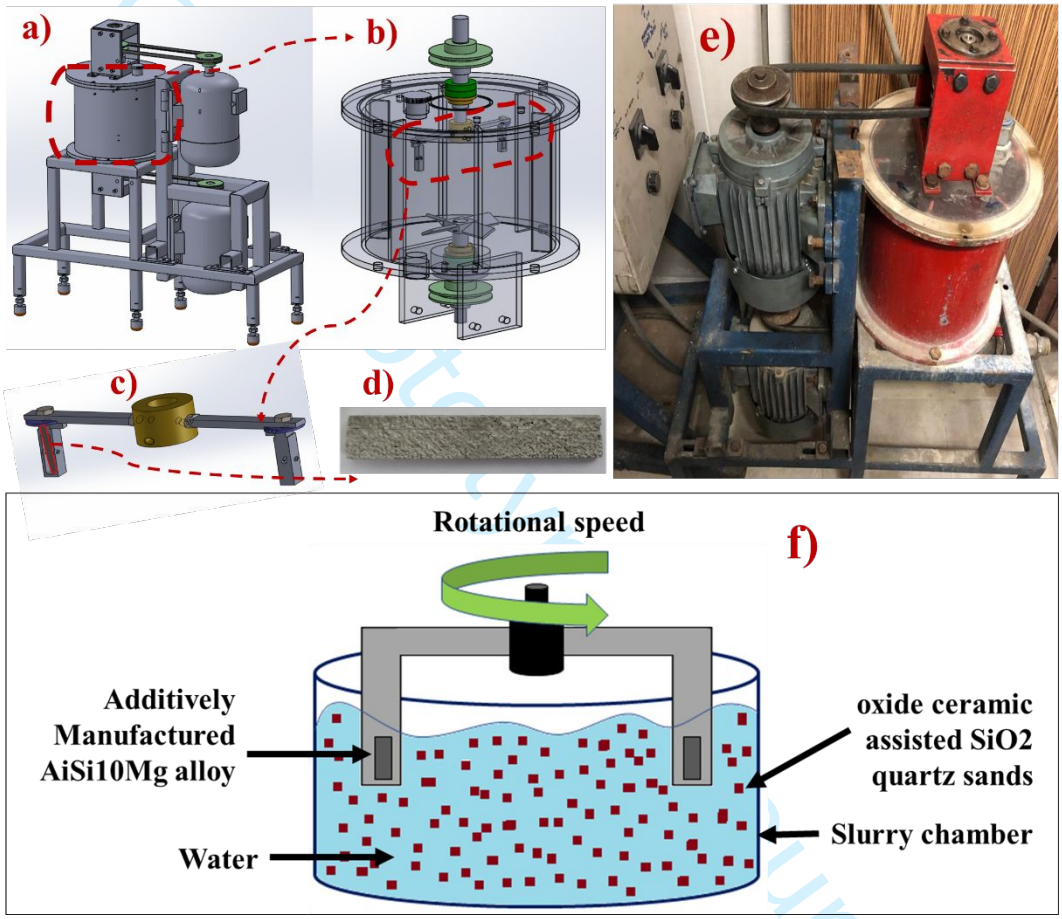

Figure 5. Test Rig, a) assembly, b) tank, c) specimen holders, d) specimen, e) whole test setup, f) slurry erosive wear mechanism

Before experiments, the samples were cleaned with tap water, dried by using a hairdryer, and weighed with a scale of 0.1 mg sensitivity. The same cleaning process was repeated after each experiment. After the samples were placed on the sample holder, they were fixed with the help of fixing bolts, not by adhesion material, contrary to the previous experiments. Since no adhesives were used, no chemicals were required to clean the samples for weighing after the test. The duration of the experiments was limited to one hour to prevent the reduction of the abrasive effect caused by the change in articulate

sizes and the sharp edge changing on the abrasive surfaces. To obtain good results, the same experiment was repeated five times and the wear values were averaged. The contact area is 1.5 cm^2 (30 x 5 mm) for each sample. After each test, the used quartz was evacuated from the system and the new quartz that had been prepared previously was included in the system. Again, after each test, the inner surfaces of the sample holders were cleaned with pressurized water to prevent any residue. (Lindsley and Marder, 1999) considered particle velocity as a critical test meter in their study and different velocities were determined as target material. They stated that the effects on them are very easily discernible and that the increase in erosive wear is obtained by increasing the speed. Besides, Desale et al. (Desale *et al.*, 2008) concluded that besides velocity and particle size, the ambient solid concentration is also an effective parameter on the erosive wear value. In this study, to examine these parameters, 3 different concentration values of sludge were prepared, three different rotation speed values, and 3 different impact angle values were used (Table 6). The rotational speed given in Table 7, corresponding to the velocity values of 1.88 m/s, 3.76 m/s, and 5.64 m/s respectively (Table 6), have been selected as 250 500 and 750 rpm. Mixer speed was kept constant as 600 rpm in the experiments. The direction of rotation of the sample and the direction of rotation of the mixer are arranged in different directions. The mixing propeller, which is used to prevent the quartz particles from settling to the bottom of the chamber, has been ensured that the mixture is uniform. In addition, the propeller blade positions are designed to move the quartz movements from the center to the chamber wall and from there upwards. During the experiment, six plates on the chamber walls prevented the quartz particles from making circular movements in the direction of sample rotation. In the experiments, besides the speed, the solid concentration was chosen as 5%, 10% and 15% at three different values. In addition, three different values were used as the impact angle as 15 °, 45 ° and 75 °. Finally, Mahr Perthometer profilometer was used for the measurement of average surface roughness values which was obtained as third time and then averaged.

Table 6. Relationship between velocity and rotational speed

Velocity [m/s]		**Rotational Speed [rpm]**
1,88	$n = \frac{60V}{2\pi R}\,[rpm]$	**250**
3,76		**500**
5,64		**750**

Table 7. Experimental Design

	Factor	Level 1	Level 2	Level 3
A	**Rotational speed (rpm)**	250	500	750
B	**Impact angle (º)**	15	45	75
C	**Concentration (%)**	5	10	15

3. Results and discussions

3.1. Weight loss evaluation

As a result of the experiments performed at different abrasive concentrations, impact angles, and speeds, the weight loss of the samples was measured. Comparisons were made on weight loss since there was no change in self-weight. Within the scope of three different tests carried out for each test condition, the wear values of a total of six samples were averaged. When the wear values are examined, it is seen that the wear values increase with the increase in the speed for all concentration and impact angle values. Among the parameters examined, the most effective parameter value is the rotational speed value and it is much more effective on weight loss compared to the impact angle and concentration parameters. (Razzaque *et al.*, 2016).

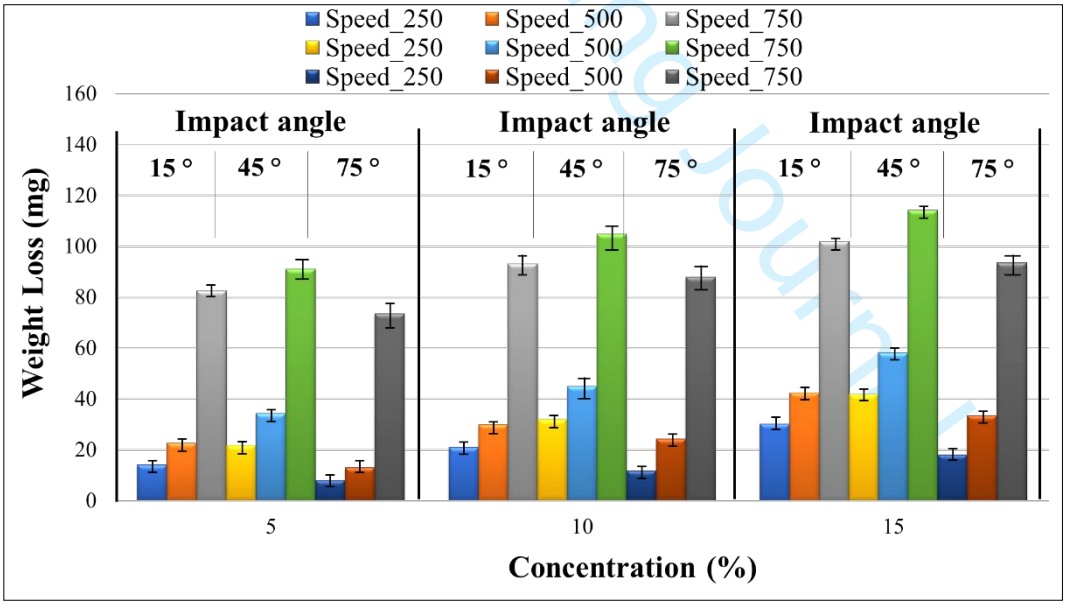

Figure 6. Weight loss under different wear conditions for 0º samples

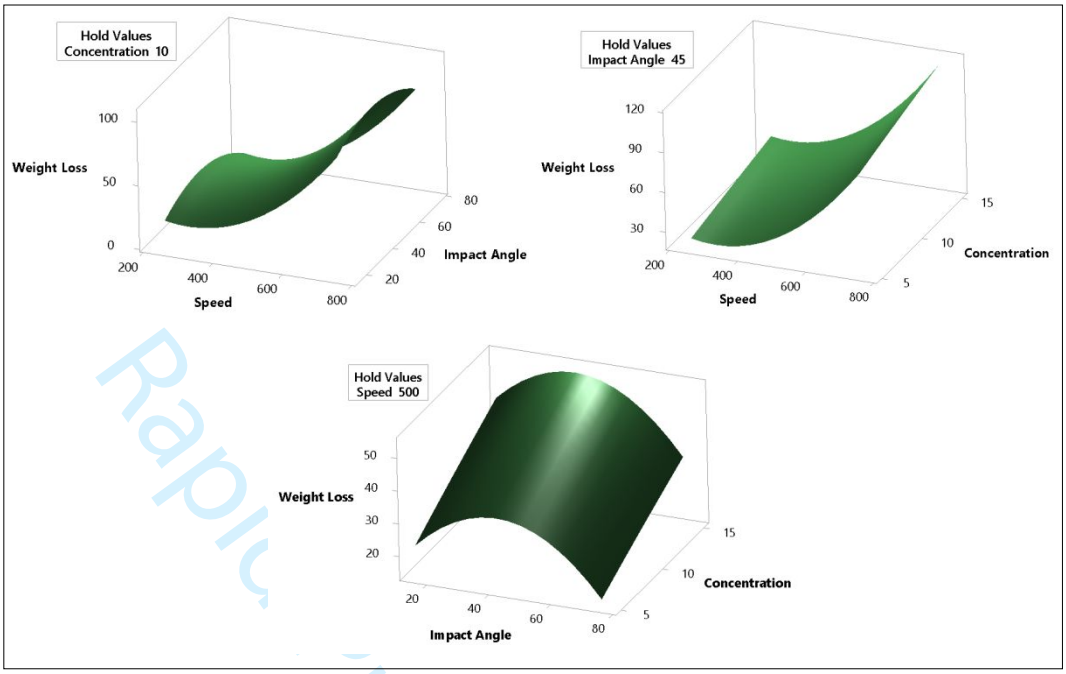

Figure 7. 3D-Weight loss graph under interactions of process parameters for 0º samples

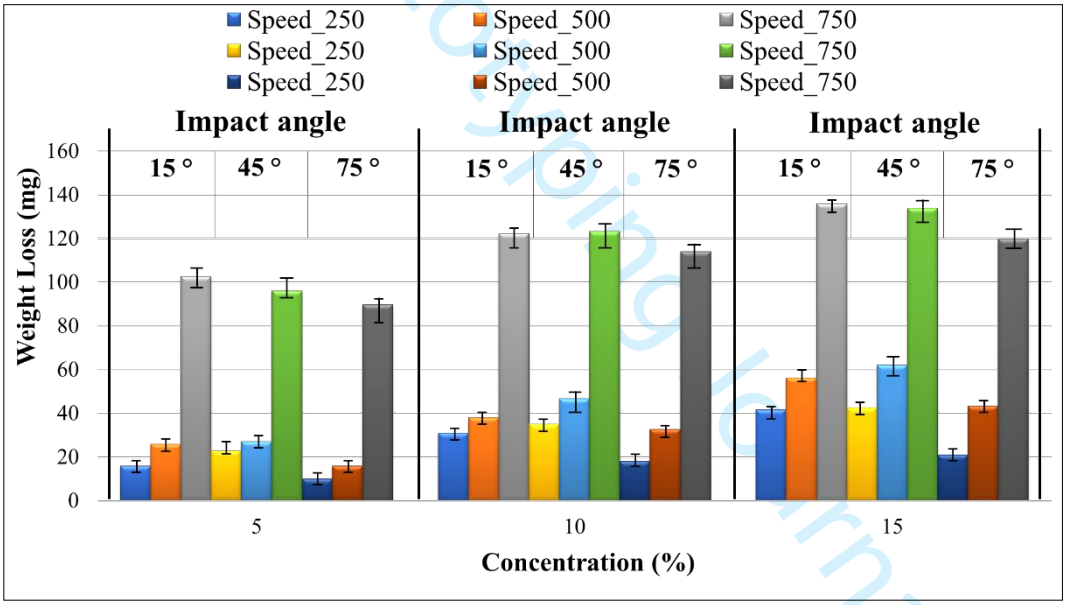

Figure 8. Weight loss under different wear conditions for 90º samples

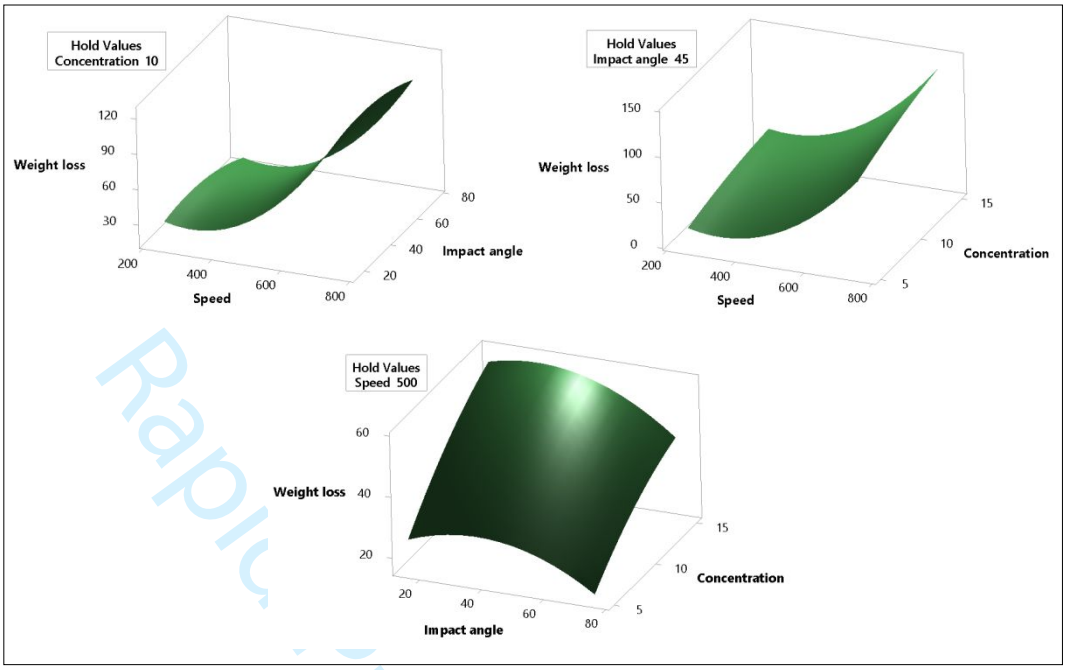

Figure 9. 3D-Weight loss graph under interactions of process parameters for 90º samples

When Figures 6 and 8 are evaluated, concerning a sample produced at 0 °, the weight loss at 250 rpm at 10% concentration and 45 ° particle impact angle is 32.8 mg, while the weight loss at 500 rpm 44.4 mg, and weight loss at 750 rpm is 104 mg. The average increases of the weight loss are 35% and 235% when the revolution speed value increases from 250 to 500 rpm and 500 rpm to 750 rpm, respectively. The increase in the amount of wear that occurs with the increase in the speed can be interpreted as the kinetic energies gained by the particles play a more effective role at high speeds. Figures 7 and 9 show that the rotational speed is the most important factor affecting weight loss of AlSi10Mg under a slurry erosive wear environment. As interpreted by Das et al. (Das *et al.*, 2006) and Mao et al. (Mao *et al.*, 2018), the wear rate in parallel with weight loss increases by increasing rotational speed. A variation of abrasive wear, erosive wear, and corrosive wear was used to describe why the behavior happened. From this point of view, it is important to select the appropriate speed in slurry pipelines by taking into account the effective role the speed plays in weight loss after a certain point. When Fig.8 is evaluated, the weight loss increased with increasing concentration values. The increase in weight loss of the specimens is mostly due to an increase in the concentration of abrasive particles in the slurry, which increases the chances of abrasive particles impinging on the specimen, resulting in increased corrosion and material removal from the surface (Rawat *et al.*, 2017; Sanman and Sreenivas Rao, 2018). Considering the

variation between impact angles at the same speed and the same concentration values, increasing the particle impact angle from 45 ° to 75 ° at 250 rpm and 5% concentration for a sample produced at 0 °, while the weight loss decreases by 552%, while the same concentration at 750 rpm. The weight loss is reduced by 126% by increasing the particle impact angle from 45 ° to 75 ° at rpm. From this, it can be concluded that the effect of the change in speed is more than the effect of the change in the angle of impact. Even at low speeds, the effect of the change in the impact angle occurs more than the effect of the angle change at high speeds. At narrow impact angles, wear is mainly due to the speed of the particle parallel to the target surface and is similar to machining done by a machine during metal cutting (Finnie and McFadden, 1978). Impact energy and particle shape can play an important role at acute angles because the angular particle shape can have a series of cutting edges that can penetrate deep into the surface with higher impact energy (Shitole *et al.*, 2015). The material loss value at 15 ° impact angle is highest at 45 ° strike angle and decreases as the strike angle increases towards the normal strike angle (Patil *et al.*, 2011). For all speed and concentration values related to the impact angles, it can be evaluated that the wear values are at 75 °, 15 °, and 45 ° impact angles, respectively, from small to large. For example, for a sample produced with 90 °, the values at 15 °, 45 ° and 75 ° for 500 rpm and 15% concentration value are 56mg, 62mg, and 43mg respectively. As can be seen, the least abrasion occurred at 75 ° and the most abrasion at 45 °.

With this study, it has been revealed that there are wear differences between the samples manufactured with a 3D printer in 0 ° and 90 ° directions. In almost all of the data obtained, especially at high speeds, with a few exceptions such as 500rpm speed, 5% concentration, and 45 ° impact angle, commonly more wear appeared for the 90 ° samples. For example, wear values for 500 rpm, 10% concentration, and 45 ° angle value for 0° and 90° directional samples are 32.7mg and 38mg, respectively. The more measured wear values in parts manufactured with 90 ° are thought to be due to the production method. It is recommended to produce 3D materials to be used in slurry pipelines at 0 ° building direction.

3.2. Surface roughness analysis

In the study, the most important criteria for slurry erosive wear were evaluated according to wear parameters of average surface roughness (Ra) based on the related studies like Xiulin et al. (Ji *et al.*, 2012) and Goyal et al. (Goyal *et al.*, 2012). With the increase in the

speed and concentration, a significant increase in surface roughness occurred. This increase can be explained by the increase in the number of particles hitting the wear surface.

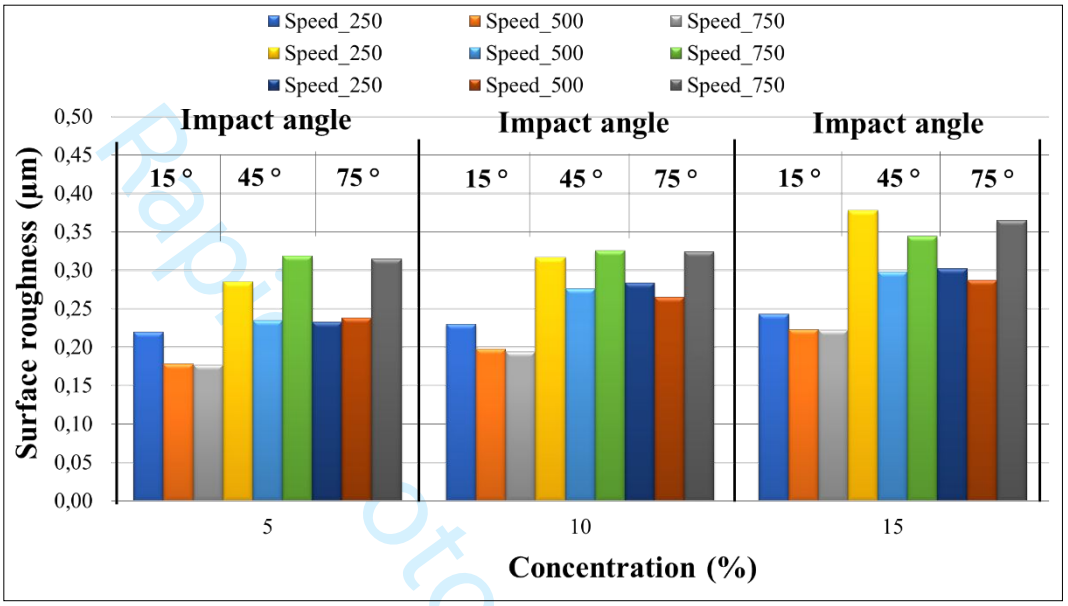

Figure 10. Surface roughness under different wear conditions for 0º samples

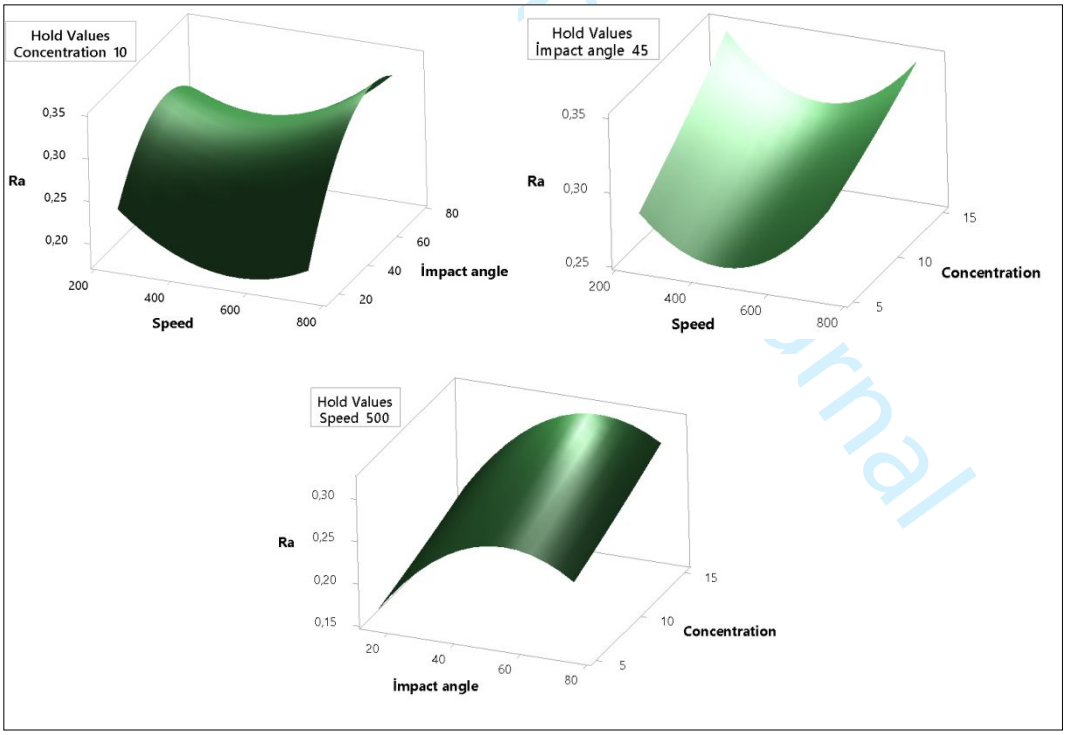

Figure 11. 3D-surface roughness graph under interactions of process parameters for 0º samples

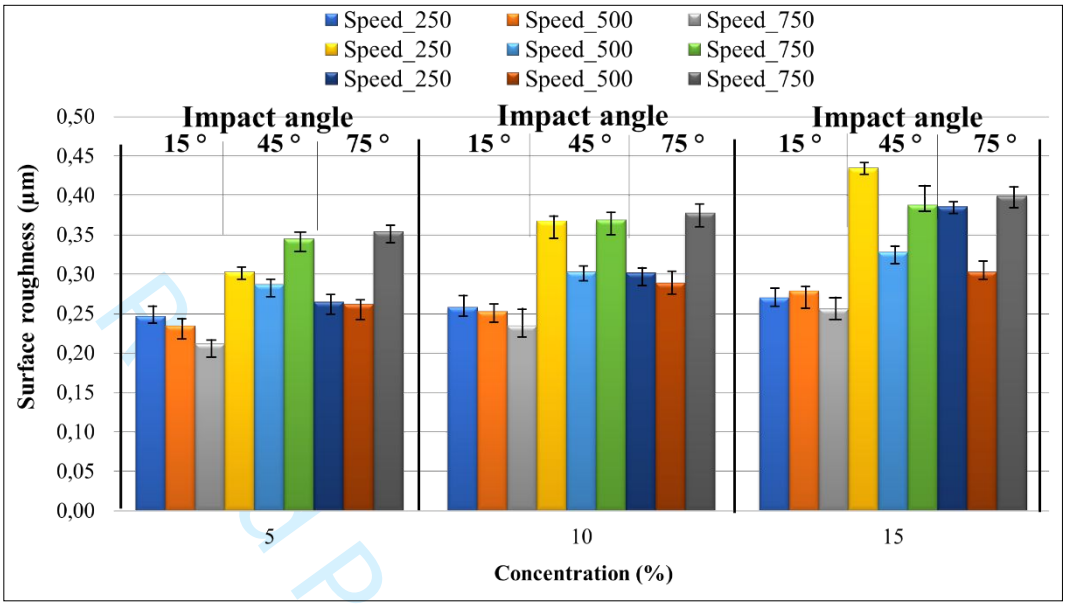

Figure 12. Surface roughness under different wear conditions for 90º samples

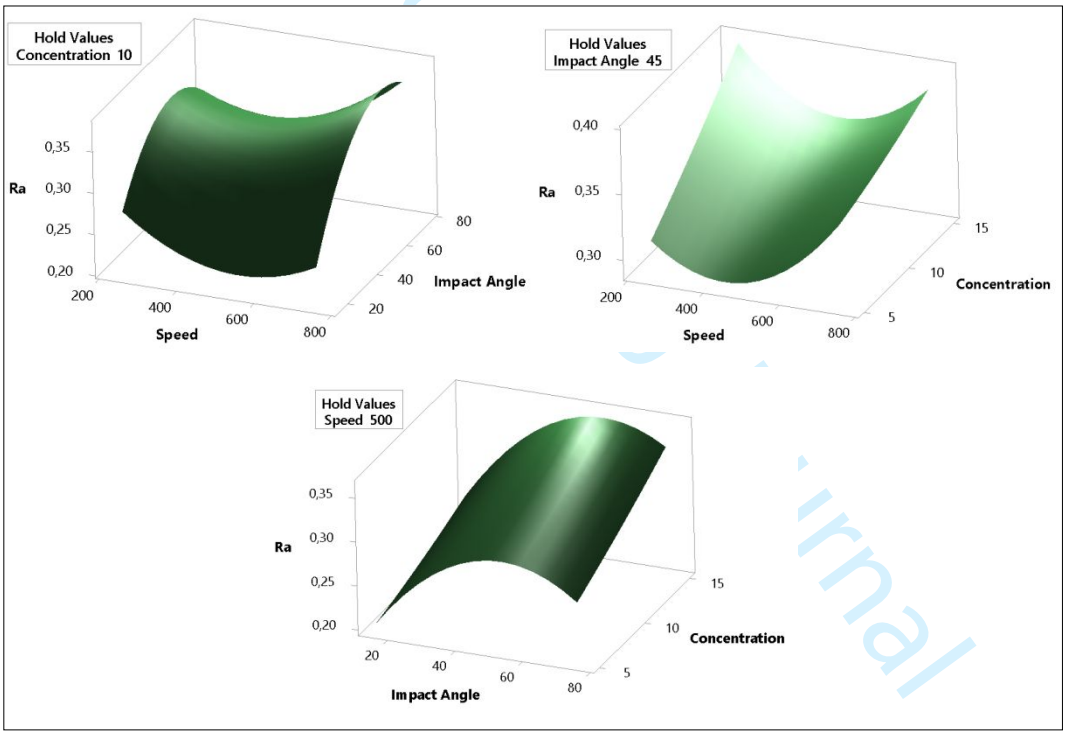

Figure 13. 3D-surface roughness graph under interactions of process parameters for 90º samples

It can be seen from Figure 10, the surface roughness values are 0.22 µm, 0.23 µm, and 0.24 µm for the 250 rpm for 0 ° sample and 5%, 10%, and 15% concentration values for the 15 ° impact angle, respectively. The increase in surface roughness by increase of quartz

concentration can be attributed to the high hardness of SiO2 quartz particles. As interpreted by Raadnui (Raadnui, 2021), this property affects the erosive wear of the propeller surface by different mechanisms. SiO2 erosive particles having higher fracture toughness generally tend to being as smaller particles and cause poor surface quality. Figures 11 and 13 show that the impact angle is the most important factor affecting the surface roughness of AlSi10Mg under a slurry erosive wear environment. As can be seen from Figures 10 and 12, the surface roughness value has the highest value at the highest concentration value. An increase in particle concentration in a multiphase flow system enhances surface damage through cutting action, scratching, and material removal (Elemuren *et al.*, 2019). Since the 75 ° impact angle is close to the 90 ° impact angle expressed as the normal impact angle in the literature, deformation wear plays a more effective role than the cutting wear. This explains the increase in surface roughness with increasing angle of impact (Desale *et al.*, 2006). For example, for 750 rpm speed and 15% concentration, the values at 15 °, 45 °, and 75 ° particle impact angles are 0.22 µm, 0.34 µm, and 0.37 µm respectively. As can be seen, the highest surface roughness value was obtained at a particle impact angle of 75 °. The wear mechanism in the SiO_2 quartz added slurry erosive wear tends to be identical to the surface wear mechanisms of micro plowing and micro-cutting. The hard SiO_2 quartz phase distribution tends to have a strong influence on the wear volume in the slurry test.

3.3. Worn surface analysis

The effect of the particle impact angle on the weight loss occurring in the material has also been proved by SEM images taken from the worn surfaces (Figure 14). The fact that the sanding marks are still present at 15 degrees indicates that there will be less deviation from the initial roughness value than other angles. By analyzing the wear difference in 0 and 90° building orientation, it is understood from the optical image (Figure 14) that the amounts of grain boundaries have changed. Due to the increase in the number of embedded particles due to the grain boundary at 0º, this increase may cause less weight loss than the 90º sample due to the loss of the main material, although it brings additional weight to the sample. Although wear losses are normally close, embedded particle additional weights may cause the difference to be overestimated.

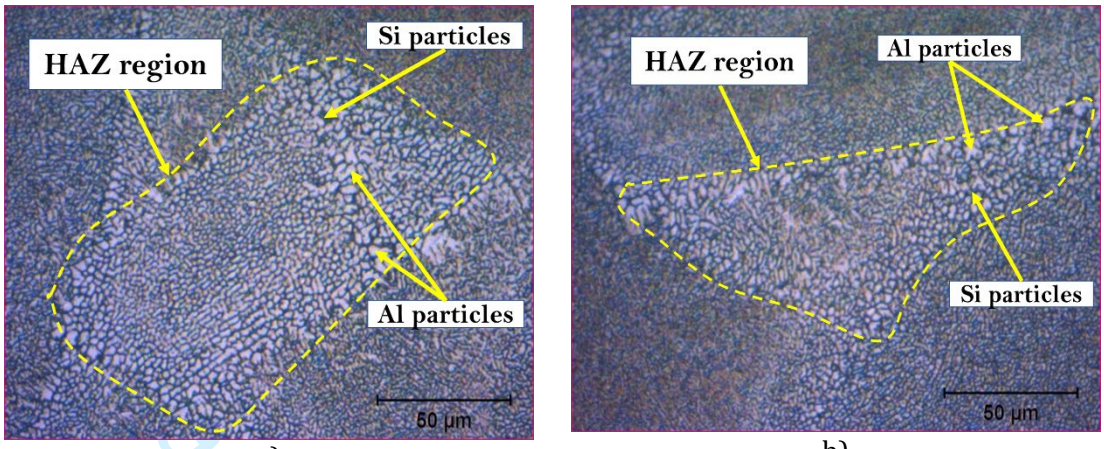

a) b)

Figure 14. Surface images after slurry erosion with building direction of, a) 0°, b) 90°

Materials processed in SLM can experience very high cooling rates of 10^6 - 10^8 K/s, which can profoundly affect the behavior of the SLMed alloy. At these cooling rates, diffusion-driven solid-state phase transformation can be completely suppressed. In addition, the formation of supersaturated solutions, non-equilibrium phases and ultrafine microstructures with very little elemental separations are possible (Yazdian *et al.*, 2010). Figure 14a and 14b show the optical images in the building directions of 0° and 90°, respectively. The geometry of the melt pool appeared crescent and irregular in shape due to the application of alternative hatching patterns. The structures of Al and Si cells in the matrix and grain boundary region, respectively, were found to be continuous in the entire melt pool region except the adjacent Heat Affected Zone (HAZ)s due to the overdispersion of Si particles near the melt pool boundary. This reveals Si morphology and appearances as idiomorphic crystals (Thijs *et al.*, 2013). The unstable SLM process presents a higher solidification rate, which further changes the phase formation, the limit of solid solubility. Rapid solidification promotes segregation of Si particles at the grain boundary where they combine with other Si particles resulting in a reduction in the total Si number. At the same time, the solid solubility of Si in Al increases, resulting in a supersaturated solution. Solubility can be further increased with varying processing parameters, promoting higher cooling rates (Lam *et al.*, 2015; Rao *et al.*, 2016).

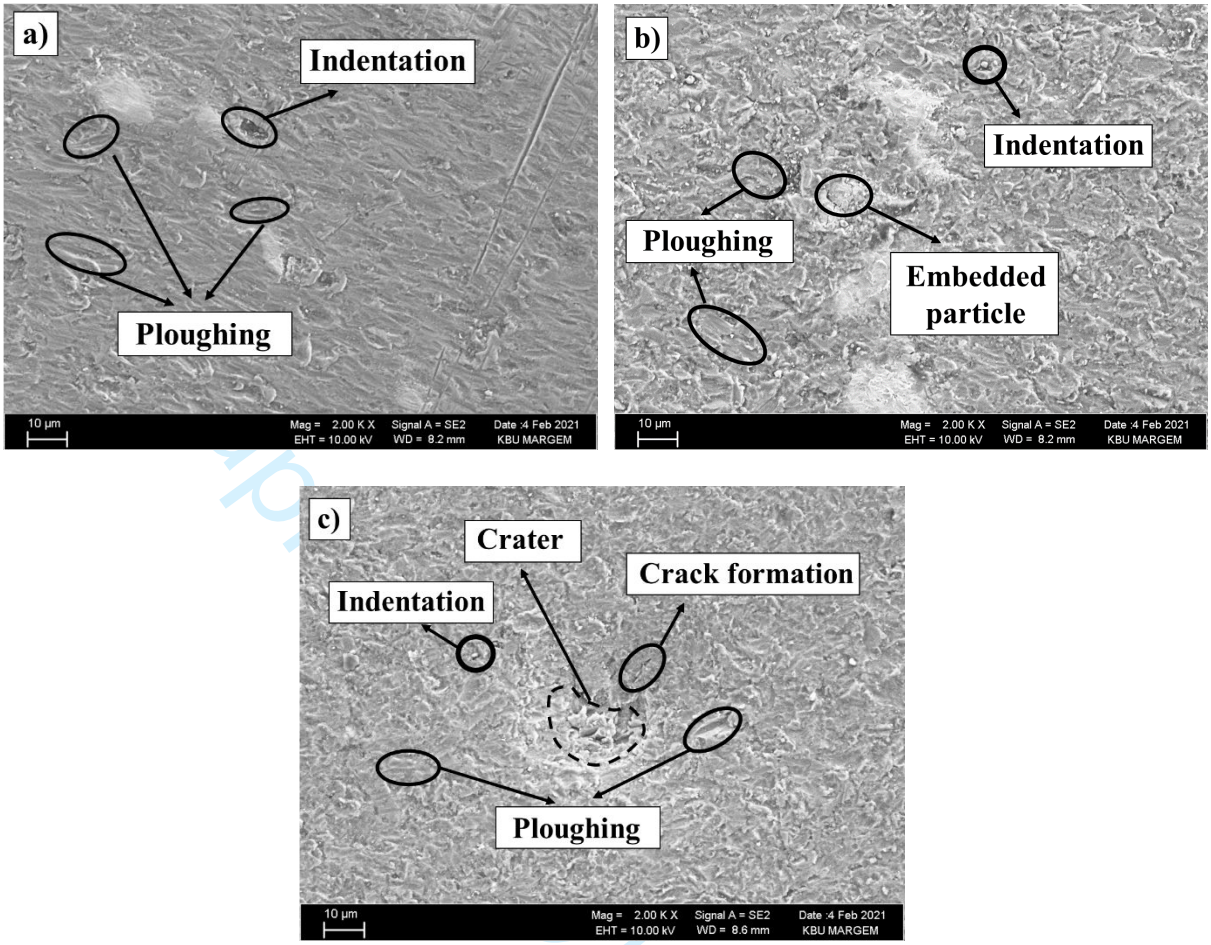

Figure 15. Surface roughness variations based on impact angle, a) 15°, b) 45° and c) 75°.

Figure 15a shows the worn surface with the lowest impact angle. This surface appears to be less worn than other surfaces as expected. Besides, when the impact angle increases, in addition to surface deformations, surface cracks caused by SiO_2 particles are also noticed. On the other hand, the excess of the roughness values on the surfaces of the material samples produced with 90 ° can be explained by the excess weight loss. As can be seen from Figures 10 and 12, surface roughness values at 750 rpm speed, 10% concentration, and 75 ° impingement angle are 0.32µm and 0.38 µm for 0 ° and 90 ° samples, respectively, with a difference of approximately 18%. Besides, the SEM images obtained for 0 ° and 90 ° samples prove that the 90 ° sample is worn more and the surface roughness is more than the 0 ° sample (Figure.16).

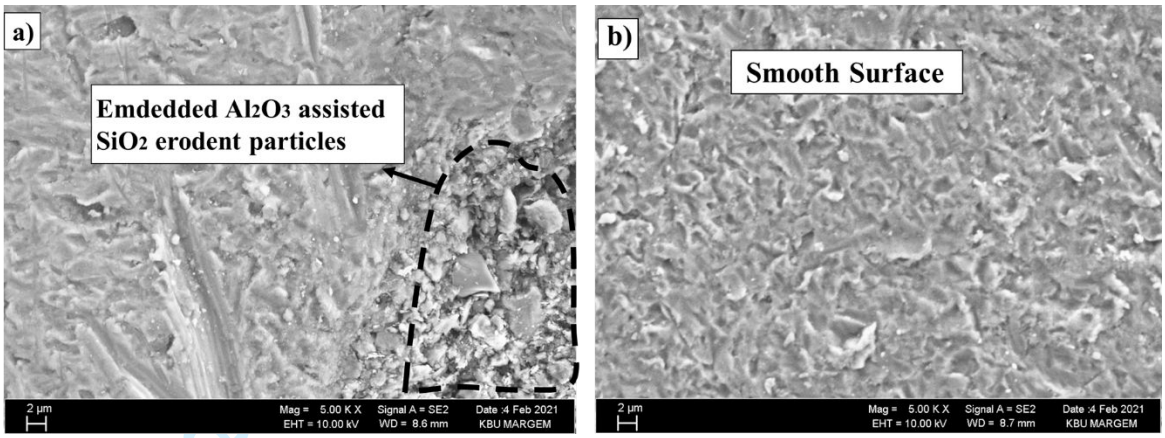

Figure 16. Worn surfaces for the rotational speed of 750 rpm, impact angle of 75º and the concentration of 15% with building direction of, a) 0°, b) 90°.

As can be seen from Figure 16, the sample with 0 ° building direction was a smooth surface, but surface microcracks were encountered. However, in the sample with 90 ° building direction, deep wear marks and surface microcracks are seen. This situation shows that the sample with a building direction of 90 cannot be able to withstand the powder building direction. The image of SiO_2 erodent particles seen in Figure 16 after slurry erosion tests are given in Figure 17 at high magnification. Here, SiO_2 particles of all sizes are encountered as expected. Finally, EDS analysis was performed on the worn image taken from a sample (Figure 18).

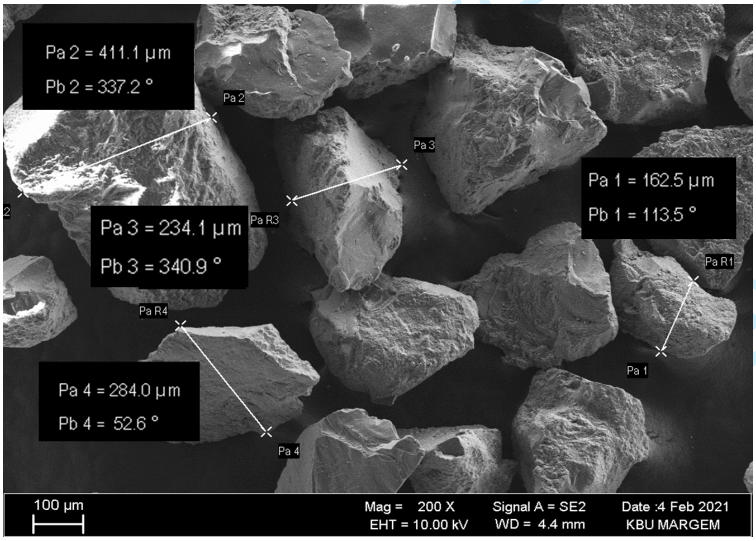

Figure 17. SEM image of quartz samples after slurry erosive test

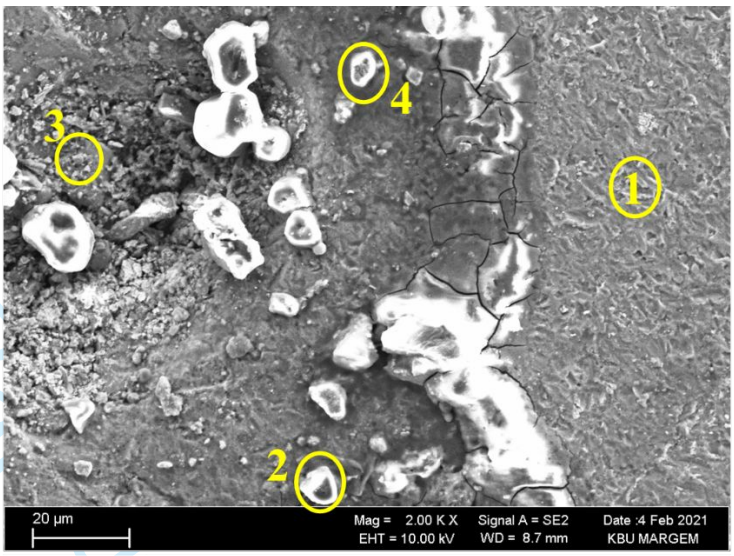

	Mass percent (%)				
Spectrum	**O**	**Mg**	**Al**	**Si**	**Mn**
1	7.15	1.08	78.47	10.53	0.38
2	73.5	1.3	1.36	0.91	0.16
3	7.85	0.73	72.27	12.5	0.04
4	17.27	1.34	66.15	10.02	0

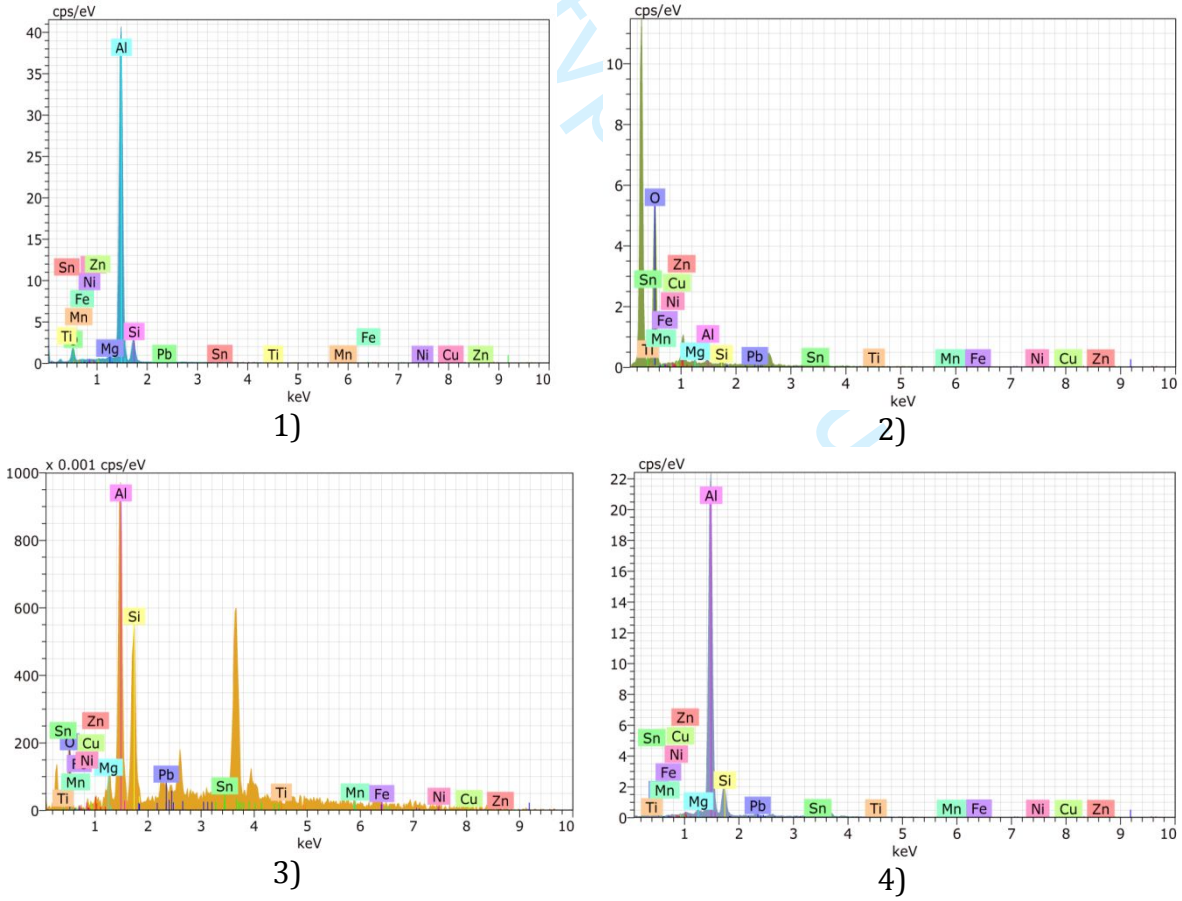

Figure 18. EDS analysis of worn surfaces of AlSi10Mg alloy with SiO_2 erodent particles

Here, zones 1 and 3 denote the AlSi10Mg alloy, and zones 2 and 4 denote SiO_2 abrasive particles, as can be understood from their Si and O ratios. This showed that the various degrees of abrasion were observed on a different region of worn surfaces of AlSi10Mg alloy. As the abrasive aspect from SiO_2 quartz is emphasized in the outer strip, more attention should be paid to decrease the risk of wear. Especially the point 2 (SiO2 erodent particle) verified itself to be an abrasive particle. General results of EDX performed on slurry erosion test samples show that the columnar composition is the same as the composition of the initial components (AlSi10Mg and SiO2). There are no steps and there is a clear difference from what the configuration is described.

4. Conclusions

This study aims to evaluate the effects of the rotational speed, impact angle, and SiO_2 concentrations on the weight loss and surface roughness during the slurry - erosive wear tests on AlSi10Mg alloy produced by additive manufacturing. Some remarkable results are summarized below.

- It is seen that the wear values increase with the increase in the rotational speed for all concentration and impact angle values.
- It is important to select the appropriate speed in slurry pipelines, taking into account the effective role the speed plays in weight loss after a certain point.
- The effect of the change in speed is more than the effect of the change in the angle of impact. Even at low speeds, the effect of the change in angle of impact occurs more than the effect of the angle change at high speeds. At narrow impact angles, wear is mainly due to the speed of the particle parallel to the target surface and is similar to machining during metal cutting.
- The least erosive wear (weight loss) occurred at 75 °, while the most occurred at 45 °.
- With the increase in the rotational speed and concentration, a significant increase in surface roughness occurred.
- Since the 75 ° impact angle is close to the 90 ° impact angle expressed as the normal impact angle in the literature, deformation wear plays a more effective role than the cutting wear.
- When the impact angle increases, in addition to surface deformations, surface cracks caused by oxide ceramics assisted SiO_2 particles are also seen.

- The sample of 90° building direction is worn more and the surface roughness is more than the sample produced at 0° building direction.
- Optimization and modelling on tribological studies can be performed for the future research about additively manufactured AlSi10Mg alloy.

References

Aboulkhair, N.T., Everitt, N.M., Maskery, I., Ashcroft, I. and Tuck, C. (2017), "Selective laser melting of aluminum alloys", *MRS Bulletin*, Vol. 42 No. 4, pp. 311–319.

Aboulkhair, N.T., Simonelli, M., Parry, L., Ashcroft, I., Tuck, C. and Hague, R. (2019), "3D printing of Aluminium alloys: Additive Manufacturing of Aluminium alloys using selective laser melting", *Progress in Materials Science*, Vol. 106, p. 100578.

Atzeni, E., Barletta, M., Calignano, F., Iuliano, L., Rubino, G. and Tagliaferri, V. (2016), "Abrasive Fluidized Bed (AFB) finishing of AlSi10Mg substrates manufactured by Direct Metal Laser Sintering (DMLS)", *Additive Manufacturing*, Elsevier B.V., Vol. 10, pp. 15–23.

Bansal, A., Goyal, D.K., Singh, P., Singla, A.K., Gupta, M.K., Bala, N., Kolte, J., *et al.* (2020), "Erosive wear behaviour of HVOF-sprayed Ni-20Cr2O3 coating on pipeline materials", *International Journal of Refractory Metals and Hard Materials*, Vol. 92, p. 105332.

Beevers, E., Brandão, A.D., Gumpinger, J., Gschweitl, M., Seyfert, C., Hofbauer, P., Rohr, T., *et al.* (2018), "Fatigue properties and material characteristics of additively manufactured AlSi10Mg – Effect of the contour parameter on the microstructure, density, residual stress, roughness and mechanical properties", *International Journal of Fatigue*, Elsevier, Vol. 117 No. April, pp. 148–162.

Ben, D.D., Ma, Y.R., Yang, H.J., Meng, L.X., Shao, X.H., Liu, H.Q., Wang, S.G., *et al.* (2020), "Heterogeneous microstructure and voids dependence of tensile deformation in a selective laser melted AlSi10Mg alloy", *Materials Science and Engineering: A*, Vol. 798, p. 140109.

Brandl, E., Heckenberger, U., Holzinger, V. and Buchbinder, D. (2012), "Additive manufactured AlSi10Mg samples using Selective Laser Melting (SLM): Microstructure, high cycle fatigue, and fracture behavior", *Materials and Design*, Elsevier Ltd, Vol. 34, pp. 159–169.

Cabrini, M., Lorenzi, S., Pastore, T., Pellegrini, S., Ambrosio, E.P., Calignano, F., Manfredi,

D., *et al.* (2016), "Effect of heat treatment on corrosion resistance of DMLS AlSi10Mg alloy", *Electrochimica Acta*, Elsevier Ltd, Vol. 206, pp. 346–355.

Chawla, N. and Shen, Y.-L. (2001), "Mechanical Behavior of Particle Reinforced Metal Matrix Composites", *Advanced Engineering Materials*, John Wiley & Sons, Ltd, Vol. 3 No. 6, pp. 357–370.

Chen, W.-B., Feng, W.-Q., Yin, J.-H. and Borana, L. (2020), "LVDTs-based radial strain measurement system for static and cyclic behavior of geomaterials", *Measurement*, Vol. 155, p. 107526.

Clark, H.M. and Llewellyn, R.J. (2001), "Assessment of the erosion resistance of steels used for slurry handling and transport in mineral processing applications", *Wear*, Vol. 250 No. 1, pp. 32–44.

Damodaran, A., Sugavaneswaran, M. and Lessard, L. (2021), "An overview of additive manufacturing technologies for musical wind instruments", *SN Applied Sciences*, Vol. 3 No. 2, p. 162.

Das, S., Saraswathi, Y.L. and Mondal, D.P. (2006), "Erosive–corrosive wear of aluminum alloy composites: Influence of slurry composition and speed", *Wear*, Vol. 261 No. 2, pp. 180–190.

Desale, G.R., Gandhi, B.K. and Jain, S.C. (2006), "Effect of erodent properties on erosion wear of ductile type materials", *Wear*, Vol. 261 No. 7, pp. 914–921.

Desale, G.R., Gandhi, B.K. and Jain, S.C. (2008), "Slurry erosion of ductile materials under normal impact condition", *Wear*, Vol. 264 No. 3, pp. 322–330.

Du, F., Zhu, J., Ding, X., Zhang, Q., Ma, H., Yang, J., Cao, H., *et al.* (2019), "Dimensional characteristics of Ti-6Al-4V thin-walled parts prepared by wire-based multi-laser additive manufacturing in vacuum", *Rapid Prototyping Journal*, Emerald Publishing Limited, Vol. 25 No. 5, pp. 849–856.

Elemuren, R., Tamsaki, A., Evitts, R., Oguocha, I.N.A., Kennell, G., Gerspacher, R. and Odeshi, A. (2019), "Erosion-corrosion of 90° AISI 1018 steel elbows in potash slurry: Effect of particle concentration on surface roughness", *Wear*, Vol. 430–431, pp. 37–49.

Fals, H.C., Lourençato, L.A., Orozco, M.S., Belém, M.J.X. and Lima, C.R.C. (2020), "Slurry erosion resistance of thermally sprayed Nb2O5 and Nb2O5+WC12Co composite coatings deposited on AISI 1020 carbon steel", *Ceramics International*, Vol. 46 No. 17, pp. 27670–27678.

Farooque, M., Zhang, A., Thürer, M., Qu, T. and Huisingh, D. (2019), "Circular supply chain management: A definition and structured literature review", *Journal of Cleaner Production*, Vol. 228, pp. 882–900.

Finnie, I. and McFadden, D.H. (1978), "On the velocity dependence of the erosion of ductile metals by solid particles at low angles of incidence", *Wear*, Vol. 48 No. 1, pp. 181–190.

Fouad, Y., El-Meniawi, M. and Afifi, A. (2011), "Erosion behaviour of epoxy based unidirectionl (GFRP) composite materials", *Alexandria Engineering Journal*, Vol. 50 No. 1, pp. 29–34.

Goyal, D.K., Singh, H., Kumar, H. and Sahni, V. (2012), "Slurry Erosive Wear Evaluation of HVOF-Spray Cr2O3 Coating on Some Turbine Steels", *Journal of Thermal Spray Technology*, Vol. 21 No. 5, pp. 838–851.

Gupta, M.K., Singla, A.K., Ji, H., Song, Q., Liu, Z., Cai, W., Mia, M., *et al.* (2020), "Impact of layer rotation on micro-structure, grain size, surface integrity and mechanical behaviour of SLM Al-Si-10Mg alloy", *Journal of Materials Research and Technology*, Elsevier, Vol. 9 No. 5, pp. 9506–9522.

Hadadzadeh, A., Amirkhiz, B.S., Li, J. and Mohammadi, M. (2018), "Columnar to equiaxed transition during direct metal laser sintering of AlSi10Mg alloy: Effect of building direction", *Additive Manufacturing*, Elsevier, Vol. 23 No. June, pp. 121–131.

Hadadzadeh, A., Amirkhiz, B.S., Odeshi, A. and Mohammadi, M. (2018), "Dynamic loading of direct metal laser sintered AlSi10Mg alloy: Strengthening behavior in different building directions", *Materials and Design*, Elsevier Ltd, Vol. 159, pp. 201–211.

Heshmat, M. and Abdelrhman, Y. (2021), "Improving surface roughness of polylactic acid (PLA) products manufactured by 3D printing using a novel slurry impact technique", *Rapid Prototyping Journal*, Emerald Publishing Limited, Vol. ahead-of-p No. ahead-of-print, available at:https://doi.org/10.1108/RPJ-09-2020-0227.

Ji, X., Yang, S., Zhao, J., Yan, C. and Liangfeng, J. (2012), "Effect of Heat Treatment on Slurry Erosion Wear Resistance of Amorphous NiP Electrodeposits", *Tribology Transactions - TRIBOL TRANS*, Vol. 55, pp. 86–90.

Junjun, L., Yunting, F., Qinghua, Z. and Joseph, S. (2018), "Green supply chain management and the circular economy: Reviewing theory for advancement of both fields", *International Journal of Physical Distribution & Logistics Management*, Emerald Publishing Limited, Vol. 48 No. 8, pp. 794–817.

Kan, W.H., Huang, S., Man, Z., Yang, L., Huang, A., Chang, L., Nadot, Y., *et al.* (2021), "Effect of T6 treatment on additively-manufactured AlSi10Mg sliding against ceramic and steel", *Wear*, Vol. 482–483, p. 203961.

Kumar, R., Antonov, M., Beste, U. and Goljandin, D. (2020), "Assessment of 3D printed steels and composites intended for wear applications in abrasive, dry or slurry erosive conditions", *International Journal of Refractory Metals and Hard Materials*, Vol. 86, p. 105126.

Kurzynowski, T., Pawlak, A. and Smolina, I. (2020), "The potential of SLM technology for processing magnesium alloys in aerospace industry", *Archives of Civil and Mechanical Engineering*, Vol. 20 No. 1, p. 23.

Lam, L.P., Zhang, D.Q., Liu, Z.H. and Chua, C.K. (2015), "Phase analysis and microstructure characterisation of AlSi10Mg parts produced by Selective Laser Melting", *Virtual and Physical Prototyping*, Taylor & Francis, Vol. 10 No. 4, pp. 207–215.

Le, V.T., Paris, H. and Mandil, G. (2017), "Process planning for combined additive and subtractive manufacturing technologies in a remanufacturing context", *Journal of Manufacturing Systems*, Vol. 44, pp. 243–254.

Li, X., Yi, D., Wu, X., Zhang, J., Yang, X., Zhao, Z., Feng, Y., *et al.* (2021), "Effect of construction angles on microstructure and mechanical properties of AlSi10Mg alloy fabricated by selective laser melting", *Journal of Alloys and Compounds*, Vol. 881, p. 160459.

Lifton, J.J., Liu, Y., Tan, Z.J., Mutiargo, B., Goh, X.Q. and Malcolm, A.A. (2021), "Internal surface roughness measurement of metal additively manufactured samples via x-ray CT: the influence of surrounding material thickness", *Surface Topography: Metrology and Properties*, IOP Publishing, Vol. 9 No. 3, p. 35008.

Lindsley, B.A. and Marder, A.R. (1999), "The effect of velocity on the solid particle erosion rate of alloys", *Wear*, Vol. 225–229, pp. 510–516.

Liu, C., Wang, Q., Cao, X., Cha, L., Ye, R. and Ramachandran, C.S. (2021), "Significance of plasma electrolytic oxidation treatment on corrosion and sliding wear performances of selective laser melted AlSi10Mg alloy", *Materials Characterization*, Vol. 181, p. 111479.

Łyczkowska, E., Szymczyk, P., Dybała, B. and Chlebus, E. (2014), "Chemical polishing of scaffolds made of Ti-6Al-7Nb alloy by additive manufacturing", *Archives of Civil and Mechanical Engineering*, Vol. 14 No. 4, pp. 586–594.

Maconachie, T., Leary, M., Zhang, J., Medvedev, A., Sarker, A., Ruan, D., Lu, G., *et al.* (2020), "Effect of build orientation on the quasi-static and dynamic response of SLM AlSi10Mg", *Materials Science and Engineering A*, Elsevier B.V., Vol. 788 No. March, p. 139445.

Manjunath Patel, G.C., Lokare, D., Chate, G.R., Parappagoudar, M.B., Nikhil, R. and Gupta, K. (2020), "Analysis and optimization of surface quality while machining high strength aluminium alloy", *Measurement*, Vol. 152, p. 107337.

Mao, L., Cai, M. and Wang, G. (2018), "Effect of rotation speed on the abrasive–erosive–corrosive wear of steel pipes against steel casings used in drilling for petroleum", *Wear*, Vol. 410–411, pp. 1–10.

Matikainen, V., Rubio Peregrina, S., Ojala, N., Koivuluoto, H., Schubert, J., Houdková, Š. and Vuoristo, P. (2019), "Erosion wear performance of WC-10Co4Cr and Cr3C2-25NiCr coatings sprayed with high-velocity thermal spray processes", *Surface and Coatings Technology*, Vol. 370, pp. 196–212.

More, S.R., Nandre, B.D. and Desale, G.R. (2014), "Development of Pot Tester to Simulate the Erosion Wear due to Solid-Liquid Mixture", *International Journal of Researchers, Scientists and Developers*, Vol. 2 No. 1, pp. 6–12.

Nurel, B., Nahmany, M., Frage, N., Stern, A. and Sadot, O. (2018), "Split Hopkinson pressure bar tests for investigating dynamic properties of additively manufactured AlSi10Mg alloy by selective laser melting", *Additive Manufacturing*, Elsevier, Vol. 22 No. April, pp. 823–833.

Ojala, N., Valtonen, K., Antikainen, A., Kemppainen, A., Minkkinen, J., Oja, O. and Kuokkala, V.-T. (2016), "Wear performance of quenched wear resistant steels in abrasive slurry erosion", *Wear*, Vol. 354–355, pp. 21–31.

Olakanmi, E.O. (2013), "Selective laser sintering/melting (SLS/SLM) of pure Al, Al–Mg, and Al–Si powders: Effect of processing conditions and powder properties", *Journal of Materials Processing Technology*, Vol. 213 No. 8, pp. 1387–1405.

Olakanmi, E.O., Cochrane, R.F. and Dalgarno, K.W. (2015), "A review on selective laser sintering/melting (SLS/SLM) of aluminium alloy powders: Processing, microstructure, and properties", *Progress in Materials Science*, Vol. 74, pp. 401–477.

Patel, S.K., Kuriachen, B., Kumar, N. and Nateriya, R. (2018), "The slurry abrasive wear behaviour and microstructural analysis of A2024-SiC-ZrSiO4 metal matrix composite", *Ceramics International*, Vol. 44 No. 6, pp. 6426–6432.

Patil, M.S., Deore, E.R., Jahagirdar, R.S. and Patil, S. V. (2011), "Study of the parameters affecting erosion wear of ductile material in solid-liquid mixture", *Proceedings of the World Congress on Engineering 2011, WCE 2011*, Vol. 3, pp. 2159–2163.

Raadnui, S. (2021), "Slurry - erosive wear and wear product analysis using a SS430 propeller", *Wear*, p. 203659.

Ramoni, M., Shanmugam, R., Ross, N.S. and Gupta, M.K. (2021), "An experimental investigation of hybrid manufactured SLM based Al-Si10-Mg alloy under mist cooling conditions", *Journal of Manufacturing Processes*, Elsevier, Vol. 70, pp. 225–235.

Rao, H., Giet, S., Yang, K., Wu, X. and Davies, C.H.J. (2016), "The influence of processing parameters on aluminium alloy A357 manufactured by Selective Laser Melting", *Materials & Design*, Vol. 109, pp. 334–346.

Rautio, T., Hamada, A., Kumpula, J., Järvenpää, A. and Allam, T. (2020), "Enhancement of electrical conductivity and corrosion resistance by silver shell-copper core coating of additively manufactured AlSi10Mg alloy", *Surface and Coatings Technology*, Vol. 403, p. 126426.

Rawat, A., Singh, S.N. and Seshadri, V. (2017), "Erosion wear studies on high concentration fly ash slurries", *Wear*, Vol. 378–379, pp. 114–125.

Razzaque, M.M., Alam, M.K. and Khan, M.I. (2016), "Effect of erodent particles on the erosion of metal specimens", *AIP Conference Proceedings*, Vol. 1754, available at:https://doi.org/10.1063/1.4958459.

Saleh, B., Jiang, J., Fathi, R., Xu, Q., Li, Y. and Ma, A. (2021), "Influence of gradient structure on wear characteristics of centrifugally cast functionally graded magnesium matrix composites for automotive applications", *Archives of Civil and Mechanical Engineering*, Vol. 21 No. 1, p. 12.

Sanman, S. and Sreenivas Rao, K. V. (2018), "Effect of sand concentration on erosive – corrosive wear behavior of chill cast aluminum – boron carbide composites", *Materials Today: Proceedings*, Vol. 5 No. 1, Part 3, pp. 2951–2954.

Shitole, P.P., Gawande, S.H., Desale, G.R. and Nandre, B.D. (2015), "Effect of Impacting Particle Kinetic Energy on Slurry Erosion Wear", *Journal of Bio- and Tribo-Corrosion*, Vol. 1 No. 4, p. 29.

Singla, A.K., Banerjee, M., Sharma, A., Singh, J., Bansal, A., Gupta, M.K., Khanna, N., *et al.* (2021), "Selective laser melting of Ti6Al4V alloy: Process parameters, defects and

post-treatments", *Journal of Manufacturing Processes*, Elsevier, Vol. 64, pp. 161–187.

Szymczyk, P., Hoppe, V., Ziółkowski, G., Smolnicki, M. and Madeja, M. (2020), "The effect of geometry on mechanical properties of Ti6Al4V ELI scaffolds manufactured using additive manufacturing technology", *Archives of Civil and Mechanical Engineering*, Vol. 20 No. 1, p. 11.

Tawfik, S.M., Nasr, M.N.A. and El Gamal, H.A. (2019), "Finite element modelling for part distortion calculation in selective laser melting", *Alexandria Engineering Journal*, Elsevier, Vol. 58 No. 1, pp. 67–74.

Thijs, L., Montero Sistiaga, M.L., Wauthle, R., Xie, Q., Kruth, J.-P. and Van Humbeeck, J. (2013), "Strong morphological and crystallographic texture and resulting yield strength anisotropy in selective laser melted tantalum", *Acta Materialia*, Vol. 61 No. 12, pp. 4657–4668.

Vargel, C. (2020), "Chapter A.1 - Historical reviews", in Vargel, C.B.T.-C. of A. (Second E. (Ed.), *Corrosion of Aluminium (Second Edition)*, Corrosion., Elsevier, Amsterdam, pp. 3–6.

Venter, A.M., Luzin, V., Marais, D., Sacks, N., Ogunmuyiwa, E.N. and Shipway, P.H. (2020), "Interdependence of slurry erosion wear performance and residual stress in WC-12wt%Co and WC-10wt%VC-12wt%Co HVOF coatings", *International Journal of Refractory Metals and Hard Materials*, Vol. 87, p. 105101.

Verma, R. (2020), "Experimental investigations on erosion of carbon steels involving textured surfaces", *Surface Topography: Metrology and Properties*, IOP Publishing, Vol. 8 No. 1, p. 15008.

Wang, M., Song, B., Wei, Q. and Shi, Y. (2019), "Improved mechanical properties of AlSi7Mg/nano-SiCp composites fabricated by selective laser melting", *Journal of Alloys and Compounds*, Vol. 810, p. 151926.

Wang, Y. and Shi, J. (2020), "Effect of hot isostatic pressing on nanoparticles reinforced AlSi10Mg produced by selective laser melting", *Materials Science and Engineering: A*, Vol. 788, p. 139570.

Waqar, S., Guo, K. and Sun, J. (2021), "FEM analysis of thermal and residual stress profile in selective laser melting of 316L stainless steel", *Journal of Manufacturing Processes*, Elsevier, Vol. 66, pp. 81–100.

Waqar, S., Liu, J., Sun, Q., Guo, K. and Sun, J. (2020), "Effect of post-heat treatment cooling on microstructure and mechanical properties of selective laser melting

manufactured austenitic 316L stainless steel", *Rapid Prototyping Journal*, Emerald Publishing Limited.

Waqar, S., Sun, Q., Liu, J., Guo, K. and Sun, J. (2021), "Numerical investigation of thermal behavior and melt pool morphology in multi-track multi-layer selective laser melting of the 316L steel", *The International Journal of Advanced Manufacturing Technology*, Springer, Vol. 112 No. 3, pp. 879–895.

Wei, P., Chen, Z., Zhang, S., Fang, X., Lu, B., Zhang, L. and Wei, Z. (2021), "Effect of T6 heat treatment on the surface tribological and corrosion properties of AlSi10Mg samples produced by selective laser melting", *Materials Characterization*, Vol. 171, p. 110769.

Wu, H., Ren, Y., Ren, J., Liang, L., Li, R., Fang, Q., Cai, A., *et al.* (2021), "Selective laser melted AlSi10Mg alloy under melting mode transition: Microstructure evolution, nanomechanical behaviors and tensile properties", *Journal of Alloys and Compounds*, Vol. 873, p. 159823.

Xi, L.X., Zhang, H., Wang, P., Li, H.C., Prashanth, K.G., Lin, K.J., Kaban, I., *et al.* (2018), "Comparative investigation of microstructure, mechanical properties and strengthening mechanisms of Al-12Si/TiB2 fabricated by selective laser melting and hot pressing", *Ceramics International*, Vol. 44 No. 15, pp. 17635–17642.

Xu, Z., Liu, A. and Wang, X. (2021), "Fatigue performance and crack propagation behavior of selective laser melted AlSi10Mg in 0°, 15°, 45° and 90° building directions", *Materials Science and Engineering: A*, Vol. 812, p. 141141.

Yazdian, N., Karimzadeh, F. and Tavoosi, M. (2010), "Microstructural evolution of nanostructure 7075 aluminum alloy during isothermal annealing", *Journal of Alloys and Compounds*, Vol. 493 No. 1, pp. 137–141.

Zhang, C., Zhu, H., Liao, H., Cheng, Y., Hu, Z. and Zeng, X. (2018), "Effect of heat treatments on fatigue property of selective laser melting AlSi10Mg", *International Journal of Fatigue*, Elsevier, Vol. 116 No. April, pp. 513–522.

Zhang, K., Liu, T., Liao, W., Zhang, C., Yan, Y. and Du, D. (2018), "Influence of laser parameters on the surface morphology of slurry-based Al2O3 parts produced through selective laser melting", *Rapid Prototyping Journal*, Emerald Publishing Limited, Vol. 24 No. 2, pp. 333–341.

Zhang, T., Li, H., Gong, H., Wu, Y., Ahmad, A.S. and Chen, X. (2021), "Effect of rolling force on tensile properties of additively manufactured Inconel 718 at ambient and

elevated temperatures", *Journal of Alloys and Compounds*, Vol. 884, p. 161050.

Zhao, X., Song, B., Fan, W., Zhang, Y. and Shi, Y. (2016), "Selective laser melting of carbon/AlSi10Mg composites: Microstructure, mechanical and electronical properties", *Journal of Alloys and Compounds*, Vol. 665, pp. 271–281.